Implantable Biomedical Devices: Wireless Powering and Communication

Anatoly Yakovlev, Sanghoek Kim, and Ada Poon, Stanford University

ABSTRACT

In recent years, there has been major progress on implantable biomedical systems that support most of the functionalities of wireless implantable devices. Nevertheless, these devices remain mostly restricted to research, in part due to limited miniaturization, power supply constraints, and lack of a reliable interface between implants and external devices. This article provides a tutorial on the design of implantable biomedical devices that addresses these limitations. Specifically, it presents analysis and techniques for wireless power transfer and efficient data transfer from both theoretical and practical standpoints. Their potential implementations are also discussed.

INTRODUCTION

In Richard Feynman's famous 1959 lecture entitled "There's plenty of room at the bottom," he presented a wild idea of ingestible surgeons where tiny surgical robots are guided through a blood vessel to the heart. Once there, the robots look around and send biological information back to an external controller. These robots were envisioned to perform local operations and even to be permanently incorporated into the body to provide continuous monitoring. The idea might sound like a science fiction dream, but in recent years there has been major progress on implantable biomedical systems that support most of the functionalities of the surgical robots. Nevertheless, these devices remain mostly restricted to research, in part due to limited miniaturization, power supply constraints, and lack of a reliable interface between implants and external devices. Much emphasis has been put on improving in vivo detection and treatment of various diseases and monitoring the physiological signals in patients. Wireless powering and communication play key roles in reducing the size, complexity, and power consumption of these devices without sacrificing robustness and functionalities. While wireless powering and communication are not new concepts, existing mechanisms do not lead to miniaturized systems. For example, most existing implants consume significant power consumption in maintaining an environmentally robust, high data rate communications link, which limits their size and performance. In [1], the authors report that increasing temporal resolution and the number of channels in cochlear implants would improve perceived sound quality in hearing-impaired patients, which requires an increase in the data rate, and consequently results in high power consumption. The number of electrodes and encoding resolution in intraocular retinal prostheses are also constrained by the achievable data rate, as stated by Liu et al. in [2]. Applications, such as cochlear implants or retinal visual prostheses, would benefit from efficient wireless powering and communication, and lead to miniature system.

One of the key limiting factors in battery-less implantable devices is the low available power associated with the wireless power link and energy harvesting circuitry. Many existing biomedical implantable devices operate in the low-MHz frequency range, such as the widely accepted 13.56 MHz industrial, scientific, and medical (ISM) band. Adhering to this frequency band not only requires large receive antennas, but also imposes difficulties in designing efficient high data rate transceivers. Our recent work has demonstrated that millimeter-sized antennas in biological tissue achieve optimal power transfer efficiency in the low-gigahertz range [3, 4]. Taking advantage of this higher frequency simplifies the design of the data link as well as the antenna and the matching network. In addition, it allows decoupled optimization of the power harvesting and telemetry circuitry, and also desensitizes the link gain to antenna orientation. The power performance of these devices can be further enhanced by implementing them in newer technology processes. For instance, recent implementation of an implantable retinal stimulator chip has been described in [5] by Luke S. Theogarajan. It was implemented in a 0.5 μm process and consumes close to 2 mW of power out of 5 V supply while operating at 714 kb/s data rate. If using a 65 nm process, the operating voltage can be reduced below 1 V, resulting in a power consumption improved by a factor of 5 or more. The power efficiency of the implantable devices can also be improved from the communications point of view. For instance, moving away from syn-

0163-6804/12/$25.00 © 2012 IEEE

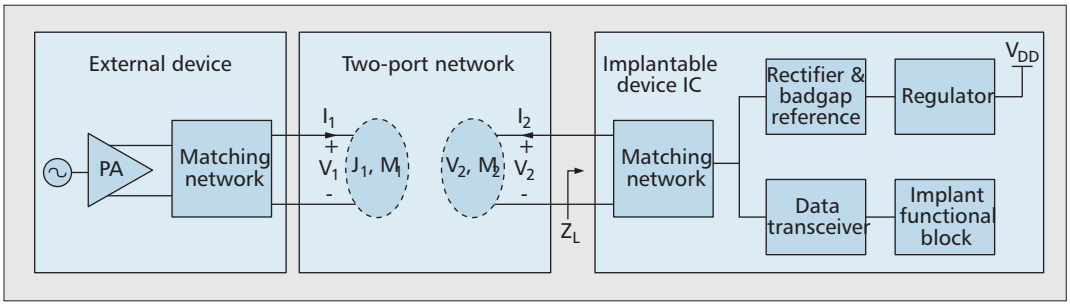

Figure 1. *Typical implantable system block diagram. The coupling between the external device and the implantable device is via a pair of antenna structures. (J_1, M_1) are the electric and the magnetic current distributions on the external antenna structure while (J_2, M_2) are those on the implant antenna structure.*

Most battery-less implantable devices consist of a matching network, rectifier, regulator, and bandgap reference. These components harvest RF power from the external device and provide a stable reference and supply voltages necessary for the device operation.

chronous modulation schemes could reduce power consumption of data transceivers from tens of picojoules per bit in today's demodulators [6] to sub-picojoule per bit.

The other design challenge of batteryless implantable devices is the low available power, which demands the use of low power on-chip circuitry, including the data transceiver, controller, and auxiliary circuitry. In this article, we will describe ways to improve the entire system efficiency, including the optimization of the external power transmitter, the implementation of the architecture, and the circuits on the implantable device. Additionally, we will emphasize the design of robust, energy efficient, and high data rate transceivers that are configurable to a wide variety of biomedical applications, such as implantable locomotive implants and bioelectric cardiac probe.

The rest of the article is organized as follows. We provide an overview of a typical implantable system. Power transfer to implantable devices in an optimal manner is discussed, followed by the discussion of forward and reverse data link, respectively. Finally, we conclude this article.

System Overview for Active Batteryless Implantable Devices

Figure 1 shows a typical active batteryless implantable system. It consists of an external device that provides power and control signals to the implantable devices, and receives sensed signals from those devices. The coupling between the external and implantable devices is via a pair of transmit and receive antenna structures, which can be modeled by a two-port network. While implants are restricted in size and power consumption, we have freedom in designing the external transmit antenna. In the next section, we explain that there is an upper limit on the power transfer efficiency that is independent of the transmitter. We also provide insights on potential transmit and receive antenna structures.

Most batteryless implantable devices consist of a matching network, rectifier, regulator, and bandgap reference. These components harvest RF power from the external device and provide a stable reference and supply voltages necessary for the device operation. In the following, we briefly describe these components and their design trade-offs.

Matching Network

A matching network is used to maximize the delivered power for a given pair of transmit and receive antenna structures. The matching network topology can be L, Π, transformer, or a higher-order matching network. The trade-offs are among bandwidth, complexity, and chip area. Since on-chip capacitors often have a much higher quality factor than inductors or bondwires in the low-gigahertz regime, a matching network using only capacitors may have a higher voltage gain and occupy smaller area than a matching network consisting of inductors or a transformer. In addition, the coupling between the transmit and receive antenna structures varies with the biological subject. The matching network can achieve improved performance if it is adaptive in real time. For example, a tunable matching is realized using a fixed inductance and a digitally controlled nine-element binary weighted capacitor array in [3]. The capacitor array is programmed based on a gradient search algorithm and improves delivered power by 3 to 6 dB.

Rectifier

The rectifier converts the AC signal to a DC voltage that can be used to supply the active circuitry in the implantable integrated circuit (IC). Depending on the received open voltage and the quality factor of the matching network, several rectifier topologies can be employed in implantable devices: diode connected metal oxide semiconductor (MOS), native MOS, and self-driven synchronous rectifier (SDSR) topologies. The critical trade-offs for these rectifier topologies are the on-resistance and reverse conduction current, which limit the efficiency of the rectifier. Typically, the RF input voltage amplitude is too low for one rectifier stage to generate sufficient voltage at the output to power up the on-chip circuitry. In this case, several charge pump-connected rectifier stages can be used to increase the output voltage to an applicable level. Compared to other rectifier topologies, SDSR configuration provides a good balance between efficiency and the input voltage at which it can operate. Moreover, the rectifier efficiency can be optimized according to its

application by adjusting the number of stages in the voltage multiplier, the capacitance per stage, and the size of transistors in each stage for a given load. [7] provides a good reference that summarizes rectifier optimization.

Regulator and Bandgap Reference

The key function of the regulator is to provide a stable supply voltage for on-chip circuitry even as the input voltage or load current experience variations. Existing regulators can be grouped into two main categories: linear regulators and switching regulators. Linear regulators are simple in design but inefficient for high drop-out voltage with large load currents. Switching regulators, on the other hand, can achieve very high efficiency, commonly over 85 percent, and can regulate to either lower, higher, or inverted output voltage as compared to its input. The tradeoff, however, is the complexity in the design of the controller, and needs for an on-chip clock and large passive components that often need to be off-chip.

Both linear and switching regulators require a stable reference voltage, which necessitates a bandgap reference circuit. Such circuits reject supply noise and are insensitive to ambient temperature by employing proportional and complementary to absolute temperature (PTAT and CTAT) components. Ueno provides an overview of sub-microwatt reference circuits that avoid the use of bipolar junction transistors or off-chip resistors in [8]. These circuits rely on MOS transistors biased in sub-threshold and linear regimes, which are particularly suitable for the application in biomedical devices because of their low power consumption.

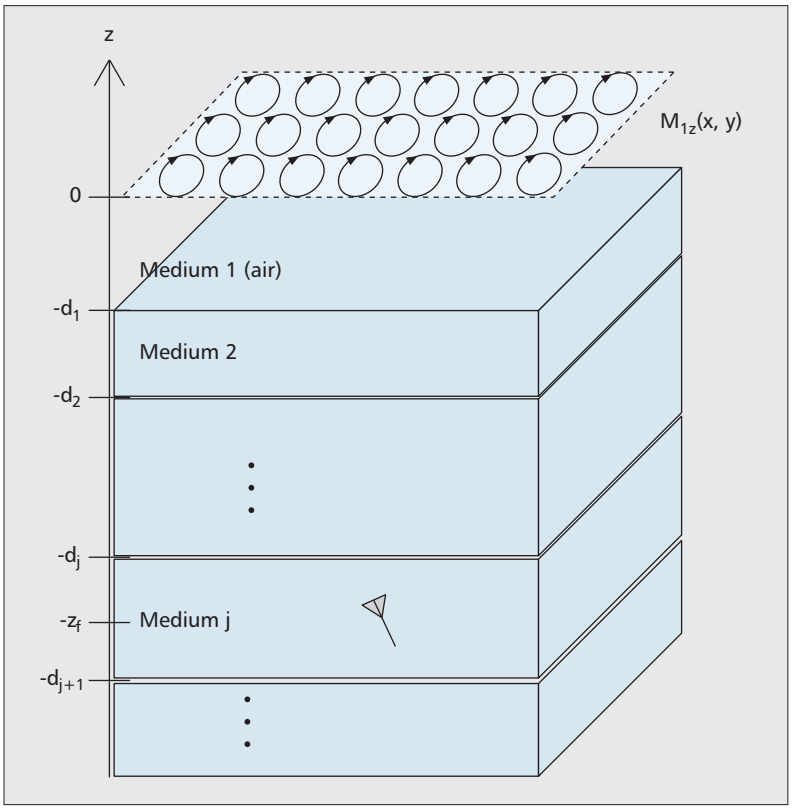

Figure 2. *A planar current source* $M_z(x, y)$ *on top of a multilayer inhomogeneous medium delivers power to an implanted antenna at* $-z_f$ *in the* j*th medium.*

Low Power Controller in the Implant Functional Block

Low power digital circuits can be designed by operating transistors at low supply voltages near subthreshold or even in deep subthreshold region. This limits the maximum operating frequency of logic gates, which, however, is adequate for many biomedical devices designed to capture low frequency physiological signals. The optimal operating condition to achieve best power efficiency for digital circuits is when leakage power equals the dynamic power. The leakage power can be further reduced by implementing Schmitt trigger logic as shown in [9], which allows the reduction of the supply voltage while maintaining robust operation.

Wireless Power Transfer into Miniature Implants

Based on full-wave analyses by considering the effects of tissue on miniature implants, we have shown that the optimal frequency for power transmission is from sub-GHz to low GHz-range, depending on the dimension of the transmit antenna [4]. The analysis in [4] used point sources to model both transmit and receive antennas, and delivered a closed-form expression, which can guide the derivation of the optimal frequency for power transfer through homogeneous tissue medium. It numerically shows that the optimal frequency depends on the dimension of the transmit antenna for power transfer through planar-layered inhomogeneous tissue media. In practice, we have freedom in designing the external transmit antenna, therefore, we need to evaluate the upper limit on power transfer efficiency of different antennas. In this section, we provide insights in how to choose optimal transmit and receive antenna structures under the respective physical constraints.

Model and Problem Formulation

We model the inhomogeneity in the link as a planar air-tissue multi-layered medium, illustrated in Fig. 2. As we aim to relax the constraints on the transmit antenna structure, we model it as an infinite sheet of arbitrary magnetic current sources. For simplicity, it can be modeled as an infinite array of infinitesimal current loops. We are interested in finding the optimal magnitude and phase for these current loops. Referring to Fig. 1, the coupling between the transmit and receive antenna structures can be modeled as a two-port network. We define the power transfer efficiency as the ratio of received power P_r at the output port to the transmit power P_t at the input port:

$$\eta = \frac{P_r}{P_t} \simeq \frac{|Z_{12}|^2}{R_{11}} \frac{R_L}{|Z_{22} + Z_L|^2} \quad (1)$$

where Z_L is the equivalent input impedance of the implantable device and R_L is its real part.

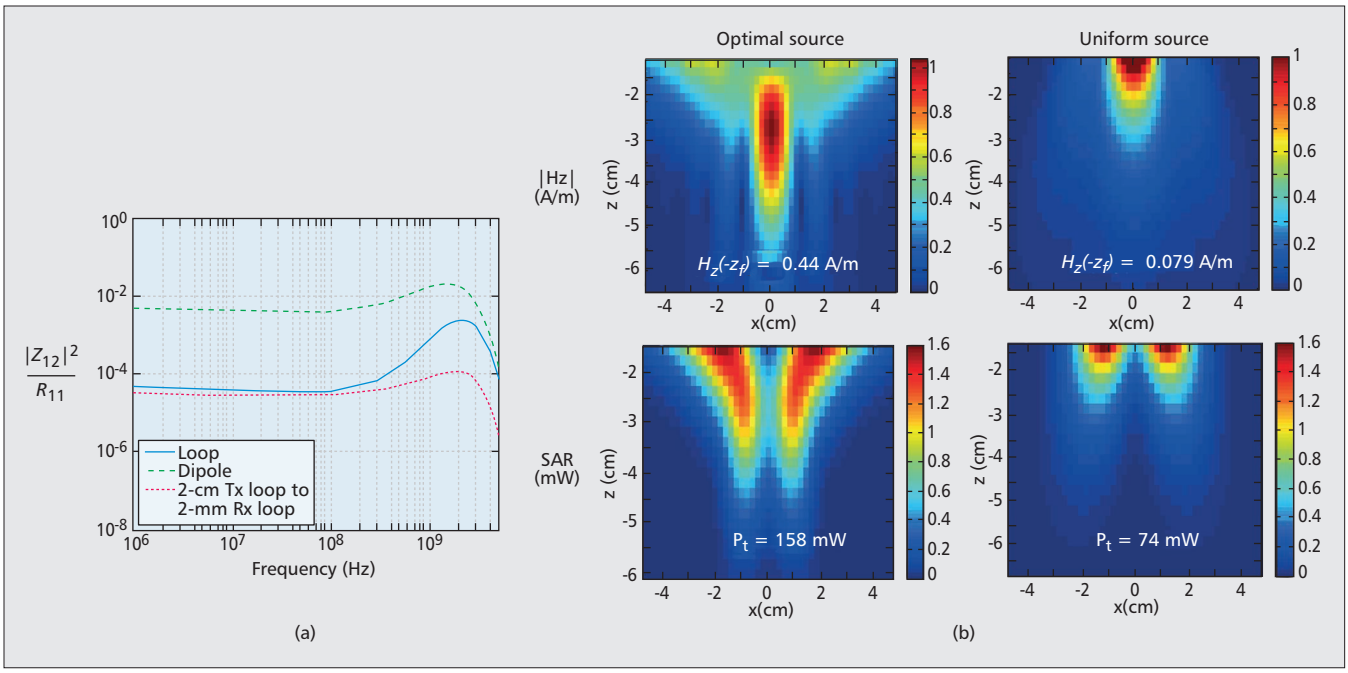

Figure 3. *a) Plots of* $|Z_{12}|^2/R_{11}$ *versus frequency for* $(d_l, z_f) = (1\text{ cm}, 5\text{ cm})$. *The upper curve plots the performance of the optimal source to a dipole, the middle curve plots that to a loop, and the lower curve plots the performance of a uniform source of 2 cm diameter to a loop. The diameter of the receive loop and the length of the receive dipole are both equal to 2 mm; b) plots the* $|\boldsymbol{H}_z|$ *and SAR distributions for the optimal source and the uniform source to a receive loop at 2 GHz. The optimal source induces much higher magnetic field than the uniform source with comparable transmit power.*

Since tissue loss usually dominates radiation loss and we assume that the transmit structure is made of perfect electrical conductor, R_{11} can be approximated from the tissue loss only. For a loosely coupled system, the first factor depends on the transmit antenna structure, while the second factor depends on the receive antenna structure and the receiver implementation. We will first optimize the transmit antenna structure for a given receiver, that is, the first factor in the above equation. Then, we will incorporate receiver constraints and choose the optimal type of receive antenna structure.

Transmitter Optimization and Focusing Effect

The optimal current distribution maximizes the mutual impedance $|Z_{21}|$ while minimizing the tissue absorption R_{11}. The detailed derivation of the optimal current distribution can be found in [10]. As a numerical example, we consider an air-muscle half space where the variation of permittivity with frequency for muscle is modeled by the 4-term Cole-Cole relaxation model [11]. When the implant is at a depth of 4 cm inside the muscle (z_f = 5 cm), Fig. 3a shows the performance of the optimal source and the uniform source to a receive dipole and a receive loop. At frequencies below 100 MHz, the performance of the optimal source is similar to that of the uniform source. At 2 GHz, however, the optimal source outperforms the uniform source by more than 10 dB. In addition, the receive dipole significantly outperforms the receive loop at low frequencies. However, the power transfer efficiency also depends on the receive antenna self-impedance R_{22} which will be discussed further.

Now, let us take a closer look at the field distribution for the receive loop at 2 GHz. Figure 3b shows the magnetic field and the specific absorption rate (SAR) distributions from the optimal and the uniform sources. The z direction of the magnetic field is plotted because the normal vector of the receive loop points along the z direction. The field strength in all plots is normalized such that the maximum SAR is 1.6 mW/cm^3 — the maximum allowable rate under the IEEE safety guidelines. As expected, the magnetic field from the uniform source is dense near the air-tissue interface, while for the optimal source there is an obvious focusing effect in the magnetic field towards the location of the receive loop. From the SAR plots, we notice that the heating effect is significant close to the tissue surface for the uniform source. For the optimal source, however, the heating effect goes deeper into the tissue without violating the safety guidelines. Consequently, the focusing effect of the magnetic field in conjunction with the diffusion effect of the electric field account for the more than 10 dB improvement in the performance of the optimal source as compared to the uniform source. Similar phenomenon has been observed for the receive dipole as well.

Power Transfer Efficiency

To complete the analysis of power transfer efficiency we need to take into account the second factor in Eq. 1. The Z_{22} is determined by the receive antenna structure, dielectric properties of surrounding medium, and the operating frequency. The Z_L depends on the equivalent input

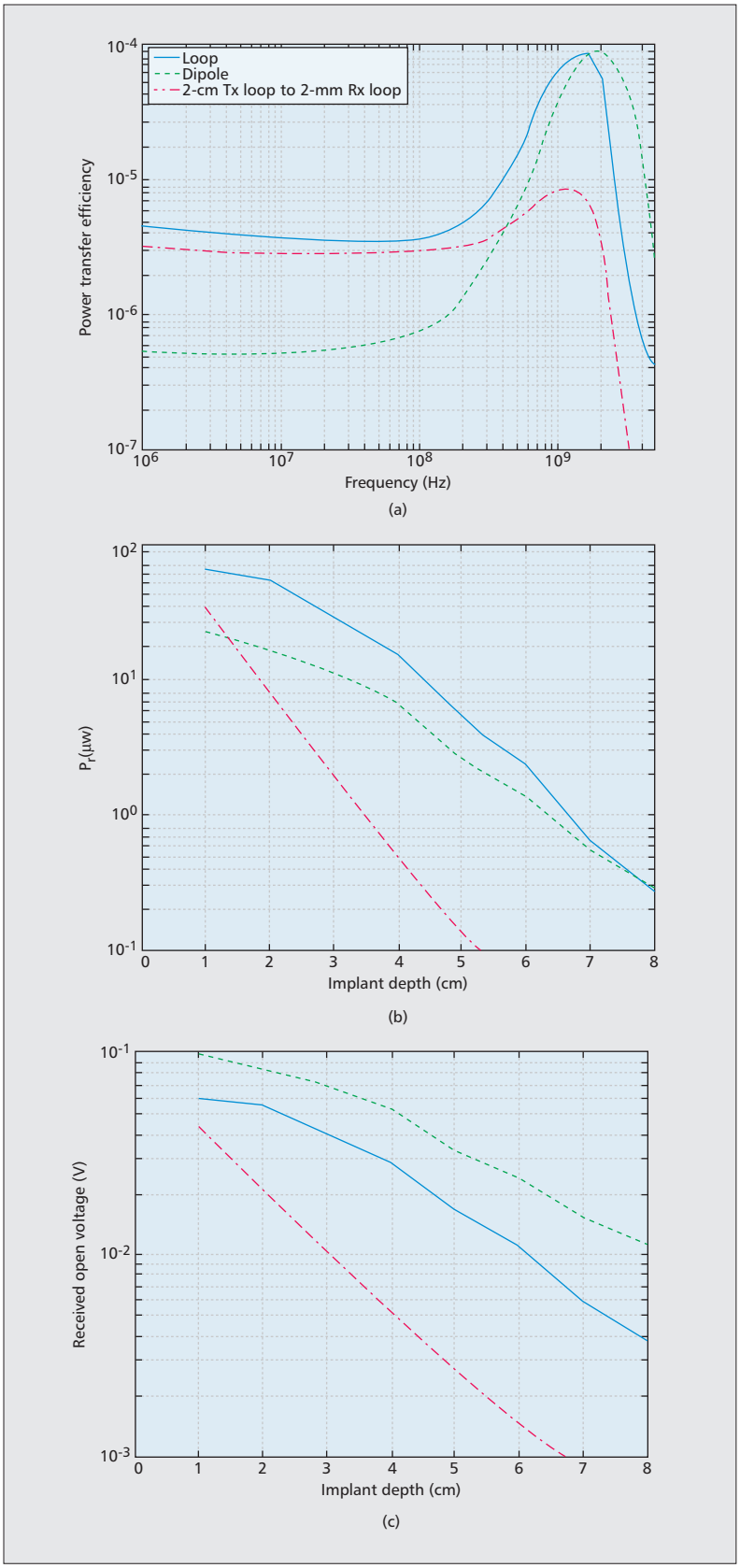

Figure 4. *The performance comparison of the optimal current source to uniform source of 2 cm diameter: a) plot of the power transfer efficiency versus frequency for* $(d_1, z_f) = (1\text{ cm}, 5\text{ cm})$*; b) received power under the SAR regulation versus the depth of implants; c) received open voltage under the SAR regulation versus the depth of implants. For (a) and (b), an equivalent input impedance of chip is 1 kΩ, Q-factor of the matching network is 10, and resonant tuned matching are assumed.*

impedance of the implant chip and the transformation ratio achieved by the matching network. The second factor in Eq. 1 is maximized when Z_L is conjugately matched to Z_{22}. However, if the equivalent input impedance differs from Z_{22} by several orders of magnitude, perfect conjugate matching is not feasible. In CMOS implementation, limited Q-factor of the matching network prevents perfect conjugate matching.

For example, Z_{22} of a small loop in the muscle medium increases from a few mΩ to hundreds of Ω as frequency varies from 1 MHz to 5 GHz. We set the equivalent input impedance of the implant chip to 1 kΩ and the Q-factor of the matching network to 10 to account for the effects of loading on power transfer efficiency in a typical CMOS implementation. Figure 4a shows the power transfer efficiency of the optimal source and the uniform source to a receive dipole and a receive loop. The power transfer efficiency is enhanced by about 10 dB via source optimization at 2 GHz. The power transfer efficiency of the receive dipole is about the same as that of the receive loop. These efficiencies are comparable because the Z_{22} of a dipole is large, varying from kΩ to tens of Ω across the frequency range of interest due to the high dielectric loss around the dipole in a lossy medium. Consequently, the power transfer efficiency of the receive dipole is worse than or comparable to that of the receive loop despite the higher $|Z_{21}|^2/R_{11}$ of the dipole.

Received Power and Received Open Voltage under SAR Regulation

It is important to consider two other metrics in wireless power transfer to implants aside from power transfer efficiency. The first metric is how much power we can deliver to the miniature implant while complying with the SAR regulation. The second metric is the received open voltage V_{oc} at the receive antenna since it has to be above certain value in order to turn on the rectifier in the implantable device IC in Fig. 1. Under the IEEE safety regulation which restricts the maximum allowable SAR, the received open voltage often determines how deep the implant can be located inside the body.

The maximum received power at the implant versus implant depth is plotted in Fig. 4b. From Fig. 4a, we observe that the power transfer efficiency is the highest in the low GHz frequencies for the deepest position of the implant. Therefore, we set the operating frequency to 2 GHz and sweep the received power versus implant depth. As before, the equivalent input impedance of the implanted chip is assumed to be 1 kΩ and the Q-factor of the matching network is 10. Figure 4c shows the received open voltage at the implant versus implant depth. Since the optimal source greatly increases the $|Z_{21}|^2/R_{11}$, it inherently improves both received power and received open voltage, and hence, increases the implant operating depth as well.

In summary, for a given receive antenna structure, implant circuitry, and antenna matching network, there is an optimal source that maximizes the power transfer performance. Adopting the optimal source greatly enhances the received power and the range of operating

depth. For the same dimension of the receive antennas, dipole antennas have advantages over loop antennas in achieving higher open voltage; an implant with a dipole antenna can operate in a deeper location than that with a loop antenna. However, due to its high dielectric loss around the antenna, the received power of a dipole antenna is worse than that of a loop antenna.

Forward Data Link

Many communication schemes for implantable devices have been demonstrated in recent literature spanning amplitude, frequency, and phase modulation, and ranging from binary to higher-order encoding in complexity. One common justification for constant amplitude modulation is the need for constant power flow since on-chip energy storage may be infeasible. This is the reason why many designers choose phase or frequency shift keying modulation over amplitude modulation. The disadvantage, however, is the need for an on-chip clock and carrier synchronization in order to receive data. Integrating synchronization circuitry in the implant receiver significantly increases power consumption, which can easily offset its advantages. Therefore, a reasonable compromise is provided by an asynchronous data link as in the case of amplitude shift keying (ASK) with data encoded in the pulse width (PW) that avoids the need for clock and carrier synchronization. In ASK-PW modulation each bit contains a transition that can be used for clock and data recovery. Figure 5d shows an equation for amplitude modulation, where m(t) represents data encoded in pulses of different duration. However, in order to maintain uninterrupted power flow to the device, the modulation depth for the ASK modulation must be low enough to provide the required average power. A high-level block diagram of an efficient ASK-PW demodulator is shown in Fig. 5a.

As mentioned earlier, for efficient data transfer on top of the power carrier, modulation depth has to be minimized. Reducing modulation depth requires a more sensitive comparator for the envelope and its average. The reference voltage is ideally set to $V_{\text{ref}} = (V_{\text{env,max}} + V_{\text{env,min}})/2$, where $V_{env,max/min}$ are the maximum and the minimum voltages of the RF envelope. However, maximum and minimum envelope voltages are not known *a priori*. Therefore, the front end of the demodulator consists of not only an envelope detector but also an envelope averaging circuit. Both implementations can be made passive by utilizing a self-synchronous rectifier topology with a small time constant for the envelope detector and a large time constant for the envelope averaging circuit. Passive envelope detector and envelope averaging circuit are shown in Fig. 5b. The envelope and its zero-crossings are extracted by a comparator that compares the envelope to its average and also acts as an amplifier that outputs a full-swing digital waveform. The resulting digital waveform can be used as a clock and is fed to a resettable integrator, which integrates the duration of the high envelope amplitude and is reset by the falling edge of the envelope. The output of the integrator is compared to a fixed threshold voltage, which is set based on the integrator time constant and the data rate requirement. Long pulses will cause the second comparator to output a digital "1," whereas short pulses will result in a digital "0." The digital data stream can be delayed and latched into memory registers using the clock waveform that was derived by the first comparator. A more detailed demodulator block diagram is shown in Fig. 5c. The modulation waveform and the output waveform of each stage of the demodulator are shown in Fig. 5e.

The key benefit of this topology is its configurability. It can operate with an adjustable modulation depth, data rate, and RF power levels. The modulation depth can be reduced by increasing the input device size of the differential pairs in the comparator to overcome the associated offset. The data rate can be adjusted by controlling the integrator time constant and the threshold voltage of the second comparator. Various RF power levels can be accommodated by controlling the resistive divider ratio $R_2/(R_1 + R_2)$ of the envelope averaging circuit. All these parameters can be designed-in if the operating conditions are known a priori or can be tuned before or during the operation by incorporating some feedback mechanism.

We have recently reported a chip that was fabricated in 65 nm standard CMOS process that utilizes this demodulation scheme [12]. The chip achieves high-Q on-chip matching network, high efficiency rectifier and regulator, and very robust asynchronous demodulator that features clock and data recovery. The demodulator achieves very competitive 0.5 pJ/bit energy efficiency and operates at very low modulation depth with up to 25 Mb/s data rate.

Reverse Data Link

Reverse data link from the implantable device to the external reader can be implemented in many different ways ranging from very complex, power hungry transmitters to simple, low-power solutions. For the first type, a dedicated transmitter with a local oscillator can be used to transmit data to the external reader. This approach allows for full-duplex communication at the cost of high complexity and power consumption. For the second type, load modulation — modulation of load impedance as seen by the antenna — can be used. Since the emphasis of this article is on low-power devices, load and backscatter modulation for the reverse link are preferable. Load can be modulated in several different ways — resistive, reactive, or a combination of the two. Depending on the link transfer function and how the load is varied, the phase and/or amplitude of the carrier will be modulated. In [13], Bletsas *et al.* provide analysis for selecting optimum load impedance that maximizes the difference between the transmitted encoded bits and thus maximizes the received signal to noise ratio (SNR) at the external reader. It is not always optimal to reflect the maximum amount of energy back to the external reader since it interferes with the power delivered to the chip. Therefore, phase modulation is a better approach for the reverse data link.

Additionally, load modulation can be easily

It is important to consider two other metrics in wireless power transfer to implants aside from power transfer efficiency. The first metric is how much power we can deliver to the miniature implant while complying with the SAR regulation. The second metric is the received open voltage at the receive antenna.

The key benefit of this topology is its configurability. It can operate with an adjustable modulation depth, data rate, and RF power levels.

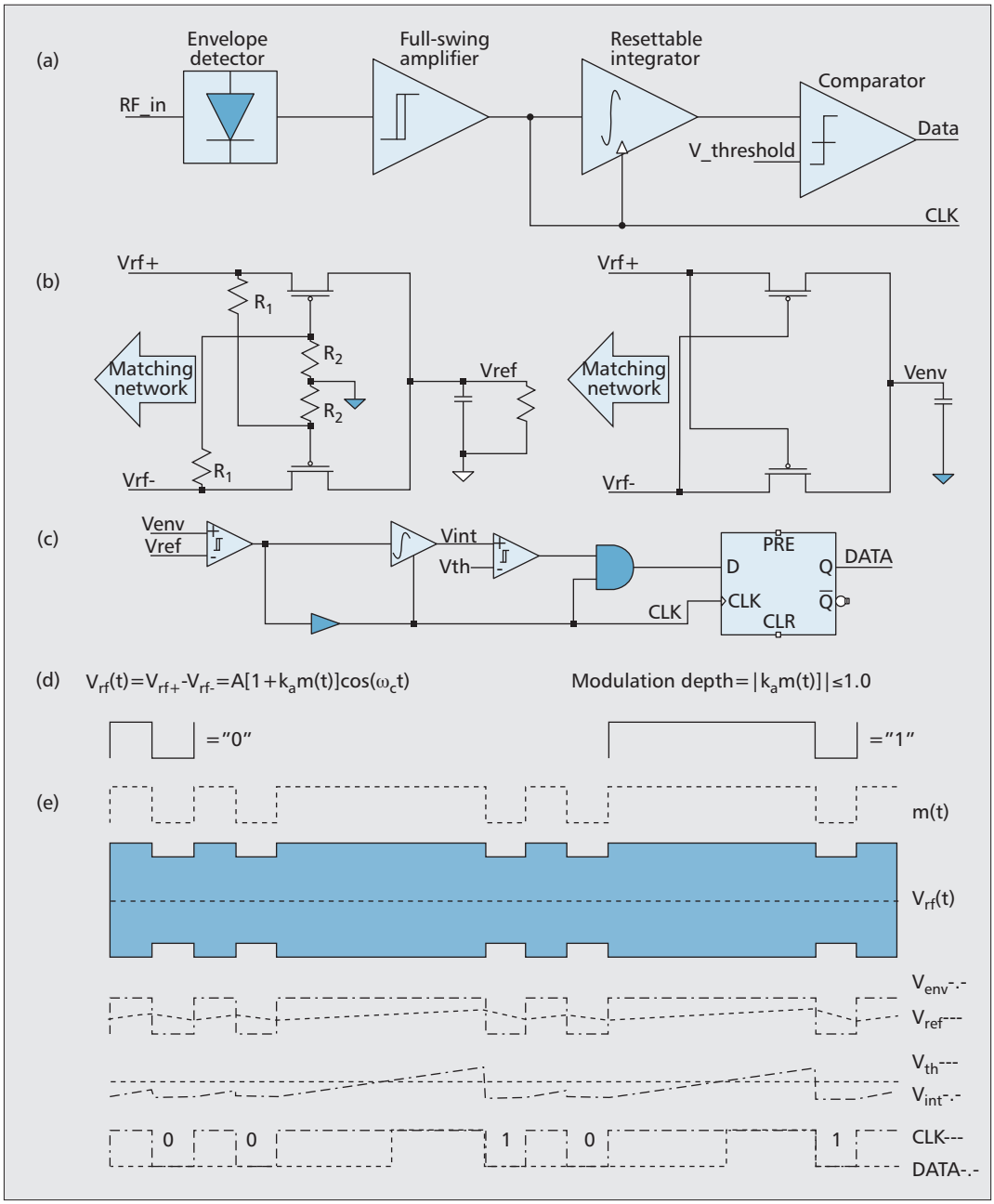

Figure 5. *a) High-level block diagram of asynchronous ASK-PWM receiver; b) passive envelope detector and envelope averaging circuit; c) detailed block diagram of ASK-PWM demodulator; d) ASK modulation equation, where m(t) represents data encoded in pulses of different duration; e) sample waveforms of modulation waveform m(t), received RF envelope $V_{rf}(t)$, output of envelope detector V_{env} and envelope averaging circuit V_{ref}, output of the integrator V_{int} compared to threshold voltage V_{th}, and data and clock waveforms.*

combined with continuous-time sensing and processing that was recently described by Schell and Tsividis in [14]. They demonstrated a system that converts an analog waveform into a digital representation without a clock or sampling. Not only does this eliminate the need for clock generation, but also saves power during idle time intervals because the signal is not sampled when there is no activity. This is perfectly suitable for a variety of biological waveforms as they tend to have long periods of low or no activity. The modulator that is driven by the event-driven sampling will only transmit data to the external reader during physiological activity and will save energy during the idle state. Since the forward link is asynchronous and does not require a clock, the event-driven sampling with load modulation minimizes power for the reverse data link by only enabling circuitry when necessary.

Conclusion

Although much work has been done in the field of wireless communications and wireless powering for biomedical implants, there is still room for improvement and optimization of the entire

system. In this article, we have presented a typical active implantable device architecture and the associated components, shown how a power link can be improved by utilizing focused powering via transmitter optimization, and provided a method for a high data rate and low power data transfer to and from the device. It is our hope that readers can find this article as an inspiration and a good starting point for their own designs.

REFERENCES

[1] J. T. Rubinstein, "How Cochlear Implants Encode Speech," *Curr. Opin.Otolaryngol. Head Neck Surg.*, vol. 12, 2004, pp. 444–48.

[2] L. Wentai *et al.*, "Image Processing and Interface for Retinal Visual Prostheses," Circuits and Systems, 2005, *ISCAS 2005, IEEE Int'l. Symp.*, vol. 3, 23–26 May 2005, pp. 2927–30.

[3] S. O'Driscoll, A. S. Y. Poon, and T. H. Meng, "A mm-Sized Implantable Power Receiver with Adaptive Link Compensation," *Tech. Dig. 2009 IEEE Int'l. Solid-State Circuits Conf.*, paper 17.5, San Francisco, Feb. 2009.

[4] A. S. Y. Poon, S. O'Driscoll, and T. H. Meng, "Optimal Frequency for Wireless Power Transmission into Dispersive Tissue," *IEEE Trans. Antennas and Propagation*, vol. 58, May 2010, pp. 1739–50.

[5] L. S. Theogarajan, "A Low-Power Fully Implantable 15-Channel *Retinal Stimulator Chip,"* IEEE J. Solid-State Circuits, vol. 43, no. 10, Oct. 2008, pp. 2322–37.

[6] A. Ghenim *et al.*, "A Full Digital Low Power DPSK Demodulator and Clock Recovery Circuit for High Data Rate Neural Implants," *IEEE Int'l. Conf. Electronics, Circuits, and Sys.*, Dec. 2010, pp. 571–74.

[7] S. Mandal and R. Sarpeshkar, "Low Power CMOS Rectifier Design for RFID Applications," *IEEE Trans. Circuits and Systems I*, June 2007.

[8] K. Ueno *et al.*, "A 300 nW, 15 ppm/C, 20 ppm/V CMOS Voltage Reference Circuit Consisting of Subthreshold MOSFETs," *IEEE J. Solid-State Circuits*, vol. 44, no. 7, July 2009, pp. 2047–54.

[9] N. Lotze and Y. Manoli, "A 62mV 0.13Wm CMOS Standard-Cell-based Design Technique Using Schmitt-Trigger Logic," *Tech. Dig. 2011 IEEE Int'l. Solid-State Circuits Conf.*, paper 19.5, San Francisco, Feb. 2011.

[10] S. Kim and A. S. Y. Poon, "Wireless Power Transfer into Miniature Implants: Transmitter Optimization," *IEEE Trans. Antennas and Propagation*, 2011.

[11] S. Gabriel, R. W. Lau, and C. Gabriel, "The Dielectric Properties of Biological Tissues: III. Parametric MODELS for the Dielectric Spectrum of Tissues," *Phys. Med. Bio.*, vol. 41, Nov. 1996, pp. 2271–93.

[12] A. Yakovlev *et al.*, "A mm-Sized Wirelessly Powered And Remotely Controlled Locomotive Implantable Device," *Tech. Dig. 2012 IEEE Int'l. Solid-State Circuits Conf.*, paper 17.6, San Francisco, CA, Feb. 2012.

[13] A. Bletsas, A. G. Dimitriou, and J. N. Sahalos, "Improving Backscatter Radio Tag Efficiency," *IEEE Trans. Microwave Theory and Techniques*, vol. 58, no. 6, June 2010, pp. 1502–09.

[14] B. Schell and Y. Tsividis, "A Continuous-Time ADC/DSP/DAC System with No Clock and with Activity-Dependent Power Dissipation," *IEEE J. Solid-State Circuits*, vol. 43, no. 11, Nov. 2008, pp. 2472–81.

BIOGRAPHIES

ANATOLY A. YAKOVLEV [S'04] got his B.S.E.E. degree from Cal Poly Pomona in 2007, where he graduated valedictorian of the School of Engineering. Between 2007 and 2008 he was with the Advanced Channel Architecture team at Western Digital. In 2009, he got his M.S.E.E. degree in analog/RF circuits from Stanford University and is now continuing to pursue his Ph.D. degree there. His Ph.D. work focuses on wireless powering and data communication for implantable biomedical devices.

SANGHOEK KIM [S'09] received his B.S. degree with a double major in electrical engineering and mathematics from Seoul National University in 2007. He received the M.S. degree in Electrical Engineering from Stanford University in 2009, where he is currently working toward a Ph.D. degree. His research interests include wireless power transfer, and biomedical applications of radio-frequency technology. He is a recipient of the Kwanjeong Educational Foundation Scholarship.

ADA S. Y. POON [S'98, M'04, SM'10] received her B.Eng. and M.Phil. degrees in electrical and electronic engineering from the University of Hong Kong, and received M.S. and Ph.D. degrees in electrical engineering and computer sciences from the University of California at Berkeley. In 2004, she was a senior research scientist at Intel Corporation. In 2005, she was a senior technical fellow at SiBeam. In 2006–2007, she was an assistant professor at the Department of Electrical and Computer Engineering in the University of Illinois at Urbana-Champaign. Since 2008, she has been at the Department of Electrical Engineering of Stanford University, where she is currently an assistant professor. Her research focuses on applications of wireless communication and integrated circuit technologies to biomedicine.

Although much work has been done in the field of wireless communications and wireless powering for biomedical implants, there is still room for improvement and optimization of the entire system. It is our hope that readers can find this article an inspiration and a good starting point for their own designs.